Crystal Structure of Alternating Ethylene−Norbornene Copolymer

Claudio De Rosa,*,† Annamaria Buono,† Finizia Auriemma,† and Alfonso Grassi‡

Dipartimento di Chimica, Università degli studi di Napoli "Federico II", Complesso Monte S.Angelo, Via Cintia, 80126 Napoli, and Dipartimento di Chimica, Università di Salerno, 84081 Baronissi (SA), Italy

Received July 2, 2004; Revised Manuscript Received September 14, 2004

ABSTRACT: Models for the crystal structure of alternating isotactic ethylene−norbornene copolymers (ENCs) are presented. Oriented fibers of ENCs samples have been obtained, and the corresponding X-ray fiber diffraction pattern has been reported. A value of the chain axis periodicity of 8.9 Å has been evaluated. A geometrical analysis and conformational energy calculations have shown that both isotactic and syndiotactic ENC chains assume nearly extended conformations having 2-fold helical **s**(2/1)*m* and glide plane **t***cm* symmetries, respectively. Both conformations account for the experimental chain axis periodicity of 8.9 Å. The crystal structure is mainly defined by the packing of the *quasi*-spherical norbornene units. The barycenters of the norbornene units are arranged on a face-centered crystalline lattice, producing a short-range three-dimensional *positional order*. Different kinds of structural disorder are present in the structure. A short-range order in the average positioning of the norbornene rings is maintained, while disorder in the positioning of the carbon atoms of the ethylene units is present. The ethylene units may assume different positions along *a* and *b* axes of the unit cell and connect with equal probability a given norbornene unit with any of its next neighbors, producing *orientational disorder* of the polymer chains as well as of the spherical norbornene units. The amount and the kind of disorder depend on the microstructure of the chains and on the condition of crystallization. The structure may be described by limit disordered models of packing, in unit cells having $a = b = 9.4$ Å and $c = 8.9$ Å or $a = 9.3$ Å, $b = 9.5$ Å, and $c = 8.9$ Å. and statistical orthorhombic or tetragonal space groups *Bmcm* or *I*4/*mmm*. The partial threedimensional order, guided by the ordered positioning of the ball-like norbornene units, is obtained even though the polymers are configurationally disordered, provided that they have a regular alternation of the comonomeric units.

Introduction

The development of metallocene catalysts has allowed the polymerization of cycloolefins via addition without ring-opening metathesis,[1−4] and a new class of polymeric materials with interesting properties have been produced. For instance, polynorbornene presents high transition and decomposition temperatures, small optical birefringence and deep ultraviolet photoresistance. These properties make this material interesting for application in microelectronic industry.[5] On the other hand, polynorbornene, and generally, polycycloolefins produced with metallocene catalysts, cannot be processed like thermoplastic polymers because the softening point is generally higher than the decomposition temperature.[1]

The unique properties of metallocene catalysts have also allowed the synthesis of ethylene−cycloolefin copolymers with different microstructures and interesting properties.[4,6−12] In particular, ethylene−norbornene copolymers (ENCs) produced with metallocene catalysts[4] are characterized by high glass transition temperature, good chemical and thermal resistance, excellent transparency and, in addition, show thermoplastic behavior. These properties make ENCs interesting thermoplastic materials suitable for high-quality applications, for instance, optical applications.[13] The main advantage of these copolymers lies in their wide-ranging glass transition temperatures, which can be set from 20 to 220 °C by varying the norbornene content in the copolymer. Moreover, the distribution of the monomers in the copolymer can be controlled from statistical to alternating.[6]

The properties of ENCs depend on the comonomer composition, the distribution of comonomers and the chain stereoregularity, which are determined by the structure of the catalyst. For these reasons ENCs have been extensively studied in the last years, especially in the effort of clarifying the microstructure of the polymer chains produced with different metallocene catalysts.[8,14,15] It is widely accepted that homo- and copolymerization of norbornene proceed by 2,3-*cis-exo* insertion, resulting in *meso*-ditactic or *meso*-atactic polymers.[16] *Ansa*-zirconocenes with C_2 and C_s symmetries produce random amorphous isotactic and syndiotactic ENCs, respectively.[4,6−12,14,15,17] Isotactic alternating ENCs have been obtained with the properly sterically hindered C_1 symmetric zirconocenes R_2C[(3-R′Cp)Flu]$ZrCl_2$,[6,9,15] (with R = methyl or phenyl, R′ = methyl or *tert*-butyl and Cp = cyclopentadienyl) and with "constrained geometry" catalysts Me_2Si(3-*tert*-BuCp)(adamantylamido)MMe_2 (with M = Zr or Hf).[18] Alternating ENCs have also been produced with other types of C_1 symmetric zirconocenes, or "constrained geometry" monocyclopentadienyltitanium amido (CpA) catalysts,[19] and, recently, by dicarbollide catalysts (η^5-$C_2B_9H_{11}$)$M(NEt_2)_2(NHEt_2)$ (M = Ti or Zr).[20,21]

The presence of crystallinity in some of ENCs produced with C_1 symmetric or CpA catalysts with melting temperatures ranging from 230 to 320 °C, dependent on the incorporation rate of norbornene,[15] has been reported. In a recent paper, we have clarified the origin of crystallinity in ENCs as due basically to the presence of alternating ethylene−norbornene sequences and, only marginally, to a stereoregular microstructure.[22] Al-

* To whom correspondence should be addressed. Telephone: ++39 081 674346. Fax ++39 081 674090. E-mail: claudio.derosa@unina.it; derosa@chemistry.unina.it.

† Università degli studi di Napoli "Federico II".

‡ Università di Salerno.

10.1021/ma0486694 CCC: $27.50
Published on Web 11/18/2004

Chart 1

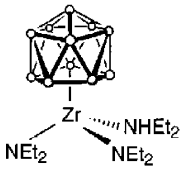

1

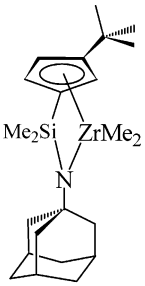

2

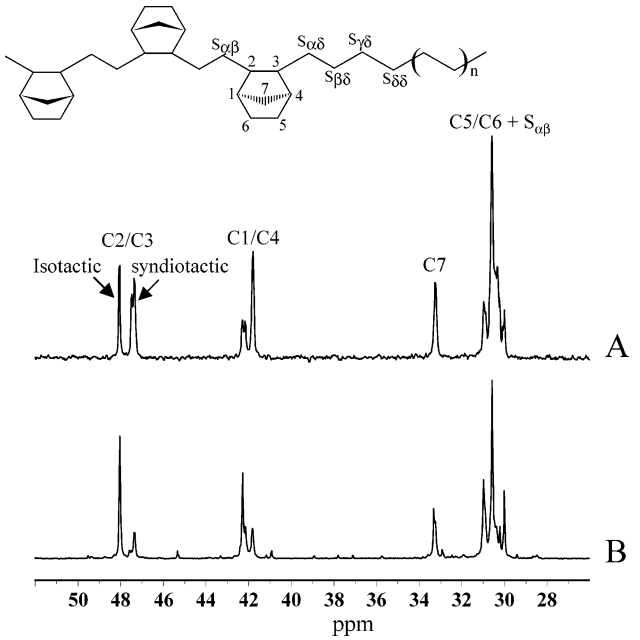

Figure 1. ^{13}C NMR spectra of ENC1 (A) and ENC2 (B) samples produced by catalysts **1** and **2** of Chart 1, respectively.[21] The assignment of resonances to carbon atoms of ethylene and norbornene units are indicated.[14]

though only a few data are available from the X-ray diffraction patterns of ENCs,[15] we have proposed a preliminary model of crystal structure defined by the packing of the *quasi*-spherical norbornene units.[22] The barycenters of the norbornene units are arranged on a face-centered crystalline lattice, producing a short-range three-dimensional *positional order*. The ethylene units may assume different positions along *a* and *b* axes of the unit cell and connect with equal probability a given norbornene unit with any of its next neighbors, producing *orientational disorder* of the polymer chains as well as of the spherical norbornene units.[22] The partial threedimensional order, guided by the ordered positioning of the ball-like norbornene units, is obtained even though the polymers are configurationally disordered, provided that they have a regular alternation of the comonomeric units.[22]

This structure represents a first example of polymeric crystals characterized by positional order and orientational disorder of the structural motif, as in "plastic" crystals of molecules having a spherical shape, for instance adamantane or norbornane.

In this paper, the crystal structure of alternating ENCs and the corresponding structural disorder are described in detail by analysis of the X-ray diffraction and conformational and packing energy calculations. Oriented fibers of ENCs are obtained and the corresponding X-ray fiber diffraction pattern is reported for the first time.

Experimental Section

Two different samples of alternating ENCs have been analyzed and characterized by X-ray diffraction. The first sample (ENC1) has been synthesized using the dicarbollide catalyst (η^5-$C_2B_9H_{11}$)Zr(NEt_2)$_2$($NHEt_2$) activated with Al^{i}Bu$_3$[20,21] (**1** in Chart 1), whereas the second one (ENC2) has been prepared with the "constrained geometry catalyst" Me_2-Si(3-*tert*-BuCp)(adamantylamido)ZrMe_2 activated with methylaluminoxane (MAO) (**2** in Chart 1).

The copolymerizations were carried out according to the procedure described in refs 20 and 21. ENC1 and ENC2 samples have a similar composition of 47 and 49.7 mol % of norbornene units, respectively, and exhibit mainly an alternating structure, as indicated by the ^{13}C NMR analysis (Figure 1).[21]

Both samples are crystalline with a similar melting temperature of 230 °C.[21]

Crystalline oriented fibers of the sample ENC1 were obtained by stretching amorphous films at 140 °C and successive annealing of the fibers at 190 °C for 30 min. The stretching was conducted with a Minimat apparatus (Rheometrics Scientific), with a strain rate of 15 mm/min. Amorphous films of the sample ENC1 were obtained by quenching the melt in liquid N_2.

Wide-angle X-ray diffraction patterns were obtained with nickel-filtered Cu Kα radiation. The diffraction patters of oriented fibers were recorded on a BAS-MS imaging plate (Fuji film) using a cylindrical camera and processed with a digital imaging reader (FUJIBAS 1800). The patterns of unoriented samples were obtained with an automatic Philips powder diffractometer.

Calculated structure factors were obtained as $F_c = (\Sigma|F_i|^2 M_i)^{1/2}$, where M_i is the multiplicity factor and the summation is taken over all reflections included in the 2θ range of the corresponding reflection peak observed in the powder profile or fiber pattern. A thermal factor $B = 8$ Å^2 and the atomic scattering factors as in ref 23 were assumed. The observed structure factors, F_o, were evaluated from the intensities of the reflections observed in the X-ray powder diffraction pattern, $F_o = (I_o/LP)^{1/2}$, where LP is the Lorentz-polarization factor for X-ray powder diffraction: $LP = (1 + \cos^2 2\theta)/(\sin^2\theta \cos\theta)$. The experimental intensities (I_o) were evaluated by measuring the areas of the peaks in the X-ray powder diffraction profile, after subtraction of the amorphous halo.

A direct comparison between the experimental X-ray powder diffraction profile and the calculated intensities was obtained calculating the X-ray powder diffraction profile ($I_{calc,2\theta i}$) from the calculated structure factors F_{hkl} of the *hkl* reflections:

$$I_{calc,2\theta i} = \Sigma|F_{hkl}|^2 MLP\Omega(2\theta_i - 2\theta_{hkl})$$

where the sum is extended over all *hkl* reflections with Bragg angles $2\theta_{hkl}$ close to the profile point $2\theta_i$ and $\Omega(2\theta_i - 2\theta_{hkl})$ is a proper profile function. A Lorentz profile function having a half-height width regulated by the average apparent crystallite sizes along *a*, *b*, and *c* axes (L_a, L_b, and L_c, respectively) was used. A good agreement with the half-height width of the peaks in the experimental profile has been obtained for $L_a = L_b = L_c = 50$ Å. This value corresponds to a coherence length along *a*, *b*, and *c* and is not a true crystallite size.

The calculations of the conformational energy have been performed on portions (four monomeric units $(EN)_4$) of isolated chains of alternating isotactic and syndiotactic ENCs. Allinger's MM2,[24] and Flory's[25] force fields were used. The nonbonded energy has been calculated by taking into account the interactions between the atoms of one monomeric unit and the atoms of other monomeric units, up to distances corresponding to twice the van der Waals distances for each pair of atoms.

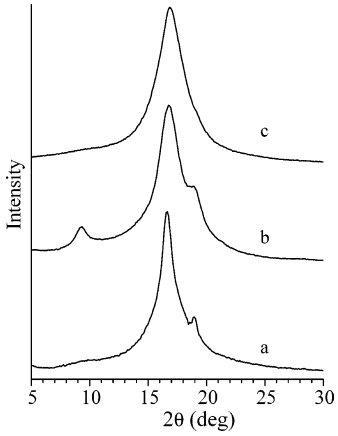

Figure 2. X-ray powder diffraction profiles of ENC1 (a) and ENC2 (b) samples and of an amorphous ENC sample (c). The amorphous sample has been obtained by quenching the melt of the ENC1 sample in liquid N_2.

The packing energy was evaluated as half the sum of the interaction energies between the atoms of one monomeric unit and all the surrounding atoms of neighboring macromolecules. The calculations of the packing energy were performed with the parameters for the nonbonded energy obtained from those reported by Flory[25] increasing the van der Waals radii by 0.15 Å, to take into account the effect of the thermal vibrations at room temperature, which tend to increase the size of the unit cell.[26] The conformation of the chain and the unit cell parameters were kept constant, and the interactions were calculated within spheres of radii equal to twice the sum of the van der Waals radii for each pair of atoms.

Results and Discussion

X-ray Diffraction. The X-ray powder diffraction profiles of as-prepared ENC1 and ENC2 samples, from catalysts **1** and **2**, respectively, are reported in Figure 2, parts a and b, respectively. The X-ray diffraction profile of an amorphous film of the sample ENC1, obtained by quenching the melt in liquid nitrogen, is reported in Figure 2c. It is apparent that the two samples ENC1 and ENC2 present similar X-ray diffraction profiles, characterized by reflections at $2\theta = 9.3$, 16.7, and 19.0° ($d = 9.5$, 5.31, and 4.67 Å, respectively) (Figure 2, parts a and b). The first sharp reflection at $2\theta = 9.3°$ in the pattern of the sample ENC2 (Figure 2b) becomes a broad peak in the pattern of the sample ENC1 (Figure 2a). These data indicate that the samples are crystalline and show a similar X-ray crystallinity. The diffraction peaks in the profiles of Figure 2, parts a and b are, indeed, much sharper than that present in the diffraction profile of the quenched amorphous sample (Figure 2c). On the other hand, both samples present a similar melting temperature of 230 °C, as evaluated from the DSC scans reported in ref 21.

The analysis of the microstructures of samples ENC1 and ENC2, by ^{13}C NMR spectroscopy, have been reported in ref 21. This analysis has indicated that the sample ENC2 is mainly isotactic because only the resonances assigned to the alternating *meso*-diisotactic structure[6,8−11,14] are observed in the ^{13}C NMR spectrum of Figure 1B. The ^{13}C NMR spectrum of the sample ENC1 of Figure 1A shows instead both resonances attributed, on the basis of the recent assignment,[14] to isotactic and syndiotactic alternating monomer pentads. Therefore, the sample ENC1, prepared with the dicarbollide catalyst **1**, presents both isotactic and syndiotactic alternating sequences with the former slightly prevailing over the latter.[21]

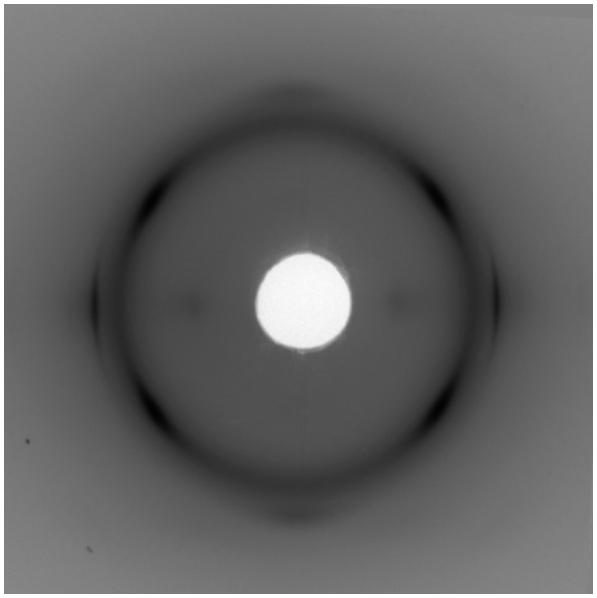

Figure 3. X-ray fiber diffraction pattern of an oriented fiber of the sample ENC1.

Table 1. Diffraction Angles 2*θ*, Bragg Distances *d*, Reciprocal Coordinates *ξ* and *ζ* and Intensities *I* of the Reflections Observed on the Layer Lines *l* of the X-ray Fiber Diffraction Pattern of Fibers of the Sample ENC1 of Figure 3, Compared with the Diffraction Angles, Bragg Distances, and Intensities Observed in the X-ray Powder Diffraction Profiles of Figure 2

fiber pattern (Figure 3)						powder profiles (Figure 2)		
2θ (deg)	d (Å)	ξ (Å^{-1})	ζ (Å^{-1})	l	I [a]	2θ (deg)	d (Å)	I [b]
9.4	9.4	0.106	0	0	vw	9.3	9.5	30
19.0	4.67	0.214	0	0	s	19.0	4.67	50
16.7	5.31	0.152	0.111	1	vs	16.7	5.31	100
19.8	4.48	0	0.223	2	n.e			

[a] Key: vs = very strong, s = strong, w = weak, vw = very weak, n.e = not evaluated. [b] Relative intensities observed in the X-ray powder diffraction profile of the sample ENC2 of Figure 2b. In the profile of the sample ENC1 of Figure 2a, the reflection at $2\theta = 9.3°$ appears as a broad halo in the range $2\theta = 8−11°$.

Despite the different ^{13}C NMR spectra and the different microstructures, the two samples ENC1 and ENC2 present similar melting temperatures and X-ray diffraction profiles, indicating that they are characterized by the same crystalline phase. Since the sample ENC2 is characterized only by isotactic sequences, we can reasonably assume that also in the ENC1 sample the crystalline phase is basically characterized by the alternating isotactic sequences. However, the crystallization of the alternating syndiotactic sequences cannot be excluded.

Crystalline oriented fibers of ENC have been obtained by stretching amorphous films of the sample ENC1 at 140 °C and successive annealing of fibers at 190 °C. The X-ray fiber diffraction pattern of fibers of the sample ENC1 is reported in Figure 3. The reflections observed in the pattern of Figure 3 are listed in Table 1, and compared with the reflections observed in the X-ray powder diffraction profiles of Figure 2.

It is apparent that also the fiber pattern of the sample ENC1 presents the same reflections observed in the powder profile of the isotactic sample ENC2. Moreover, the fiber pattern clearly shows that the peak of strong intensity observed at $2\theta = 16.7°$ in the powder profiles

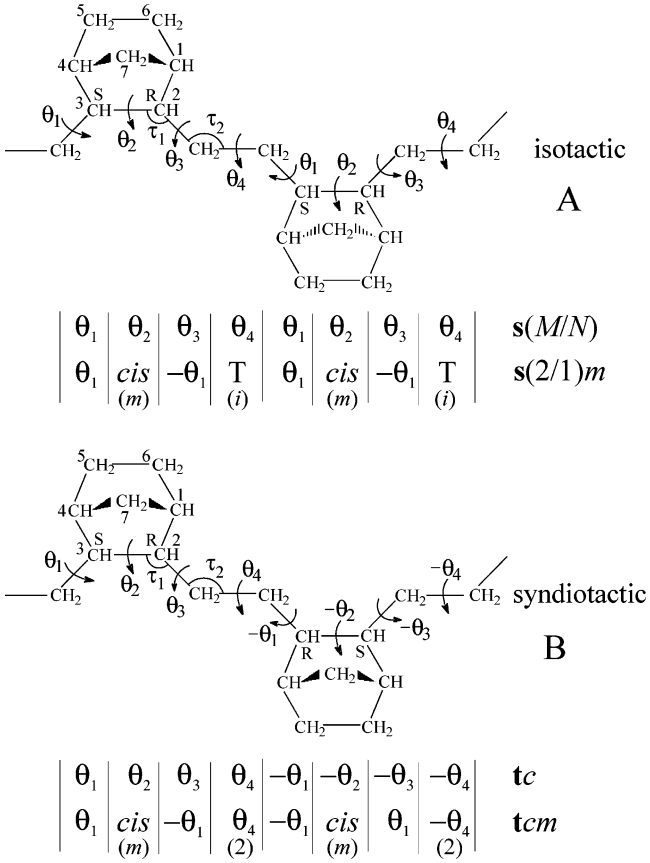

Figure 4. Line repetition symmetry groups and corresponding sequences of torsion angles for chains of *meso*-isotactic (A) and syndiotactic (B) alternating ethylene−norbornene copolymers. The position of mirror planes (*m*), binary axes (2), and inversion centers (*i*) along the polymer chain are also indicated.

of Figure 2 corresponds to a first layer line reflection (Figure 3 and Table 1). From the X-ray fiber diffraction pattern a value of the chain axis periodicity of 8.9 Å has been evaluated. It is also worth noting from Figure 3 that the diffuse background scattering appears as a continuous, smooth function over all reciprocal space and remains constant up to high values of 2θ. Indeed, there is no evidence of the presence of maxima in the background scattering and of streaks of the Bragg reflections.

Geometrical Analysis. The copolymerization of ethylene with norbornene proceeds via 2,3-*cis*-*exo* insertion of the norbornene units, resulting in *meso*-ditactic or *meso*-atactic microstructures.[16] The configuration of carbon atoms C2/C3 in a norbornene ring can be only *R*/*S* or *S*/*R* (Figure 4). Depending on configurations in two successive norbornene rings, *meso*-diisotactic and *meso*-disyndiotactic polymers are possible.

The conformation of the chain in the crystalline state may be defined, using the equivalence principle,[27] in term of its symmetry, which must be compatible with the chemical constitution and configuration. The possible line repetition groups for ENC chains compatible with the isotactic or syndiotactic configurations are reported in Figure 4. The helical repetition is compatible only for the isotactic chain; the line repetition group is **s**(*M*/*N*) and corresponds to a succession of torsion angles $(\theta_1\theta_2\theta_3\theta_4)_n$ (Figure 4A). The glide plane repetition is instead compatible for the syndioactic chain, the line repetition group being **t***c*, corresponding to a succession of torsion angles $(\theta_1\theta_2\theta_3\theta_4-\theta_1-\theta_2-\theta_3-\theta_4)_n$ (Figure 4B). Both *meso*-isotactic and syndiotactic polymer chains may present mirror planes perpendicular to the chain axis, crossing the C2−C3 bond of the norbornene ring (Figure 4). Inversion centers in the middle of the CH_2-CH_2 bond of the ethylene units may be present only for the isotactic chain (Figure 4A), whereas binary axes crossing the same bond and perpendicular to the chain axis may be present for the syndiotactic chain (Figure 4B). As a consequence, line repetition groups **s**(*M*/*N*) and **s**(2/1)*m* are possible for the *meso*-isotactic chain (Figure 4A), whereas the **t***c* and **t***cm* line repetition groups are possible for the *meso*-syndiotactic chain (Figure 4B).

In the case of the syndiotactic chain, if mirror planes perpendicular to the chain axis, bisecting the C2−C3 bonds, and binary axes perpendicular to the chain axis, crossing the CH_2-CH_2 bond of the ethylene units, are both present, a conformation of the kind $(\theta_1\ cis-\theta_1\ \theta_4\ -\theta_1\ cis\ \theta_1\ -\theta_4)_n$ is produced and the chain degenerates in a cycle (Figure 4B). However, if $\theta_1 = T = 180°$ and $\theta_4 = T = 180°$, or slightly deviated from 180°, extended and straight chains are obtained with the right values of the bond angles.

The **s**(2/1)*m* symmetry of the isotactic chain corresponds to a succession of torsion angles $(\theta_1 cis-\theta_1 T)_n$ (Figure 4A), whereas the **t***cm* line repetition group corresponds to a succession $(\theta_1\ cis-\theta_1\ \theta_4-\theta_1\ cis\ \theta_1\ -\theta_4)_n$ (Figure 4B). The value of the experimental chain periodicity $c = 8.9$ Å of ENCs, found by X-ray fiber diffraction, suggests nearly extended chains with a repetition occurring after two monomeric EN units. This is compatible with the **s**(2/1)*m* symmetry for the isotactic chain, and **t***c* or **t***cm* line repetition groups for the syndiotactic chain.

Conformational Energy Analysis. Conformational energy calculations have been performed on portions of isolated *meso*-isotactic and syndiotactic chains as those shown in Figure 4, but made of four monomeric EN units, by application of the equivalence principle[27] to successive constitutional units, assuming general line repetition groups **s**(*M*/*N*) and **t***c* for isotactic and syndiotactic chains, respectively. As a consequence, the sequences of the torsion angles in the main chain are of the kind $(\theta_1\theta_2\theta_3\theta_4)_n$ for the isotactic chain (Figure 4A) and $(\theta_1\theta_2\theta_3\theta_4-\theta_1-\theta_2-\theta_3-\theta_4)_n$ for the syndiotactic chain (Figure 4B).

We have calculated maps of the conformational energy as a function of the two torsion angles θ_1 and θ_3 (Figure 4), assuming $\theta_2 = cis = 0°$ and $\theta_4 = trans = 180°$, for both isotactic and syndiotactic chains. The latter condition arises from the need to consider only the possible conformations assumed in the crystalline state and produces sufficiently extended conformations, which can be packed in a crystalline lattice for each value of the torsion angles θ_1 and θ_3. The maps have been calculated for a fixed conformation of the norbornene rings and for fixed values of the bond angles. The conformation of the norbornene rings has been assumed as that found in model compounds, as in 2,3-substituted norbornene.[28] The geometrical parameters assumed in the present calculations are reported in Table 2. Maps of the conformational energy as a function of θ_1 and θ_3 are reported in Figure 5, parts A and B, for the isotactic and syndiotactic ENC chains, respectively.

It is apparent that for both isotactic and syndiotactic chains minima of the conformational energy are localized in the regions corresponding to θ_1 and θ_3 close to 180° (Figure 5). For the isotactic chain the minimum is

Table 2. Values of the Bond Lengths and Bond Angles Used in the Calculations of the Conformational Energy Maps of Isotactic and Syndiotactic ENC Chains of Figure 5[a]

Bond Lengths (Å)			
C−C	1.54	C−H	1.10

Bond Angles (deg)			
C1−C2−C3 ≡ C2−C3−C4	103.1	C3−C4−C7 ≡ C5−C4−C7	101.5
C4−C5−C6 ≡ C5−C6−C1	103.1	C2−C1−C7 ≡ C6−C1−C7	101.5
C1−C7−C4	94.4	C−C−H	109.5
τ_1 = CH−CH−CH_2	116.0	H−C−H	108.0
τ_2 = CH_2−CH_2−CH	114.0		

[a] The labels of the carbon atoms and the definitions of the backbone bond angles τ_1 and τ_2 are given in Figure 4.

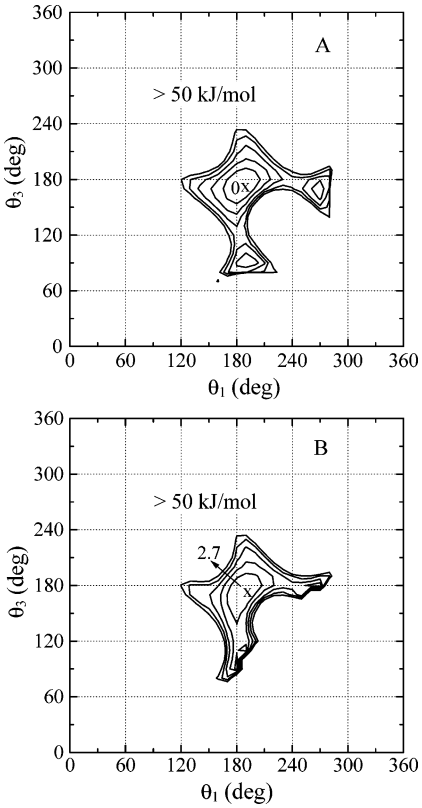

Figure 5. Maps of the conformational energy as a function of the torsion angles θ_1 and θ_3, with $\theta_2 = 0$ and $\theta_4 = 180°$, for isotactic (A) and syndiotactic (B) ENC chains. Line repetition symmetries **s**(*M*/*N*) and **t***c* are assumed for the isotactic and syndiotactic chains, respectively. The curves are reported at intervals of 10 kJ/mol of monomeric units with respect to the absolute minimum of the map A assumed as zero. The value of the energy of the minimum of the map B, with respect to the absolute minimum, is also reported.

obtained for slight opposite deviations of θ_1 and θ_3 from 180° ($\theta_1 = -\theta_3 = -174.6°$) (Figure 5A), corresponding to a succession of torsion angles (θ_1 *cis*−θ_1 T)$_n$ and line repetition group **s**(2/1)*m*. The chain periodicity calculated for this conformation is c = 8.86 Å according to the experimental chain axis.

For the syndiotactic chain the energy minimum is also obtained for $\theta_1 = -\theta_3 = -174°$ (Figure 5B), corresponding to a sequence of torsion angles (θ_1 *cis*−θ_1 *T* −θ_1 *cis* θ_1 *T*)$_n$. In this case a map of the conformational energy has also been calculated as a function of θ_1 and θ_4, assuming $\theta_1 = -\theta_3$ and $\theta_2 = 0$. The lowest energy minimum (only 1 kJ/mol higher than the energy minimum of the isotactic chain of Figure 5A) has been obtained for $\theta_1 = -176°$ (T^-) and $\theta_4 = 170°$ (T^+), with the torsion angle θ_4 slightly deviated from 180° and a

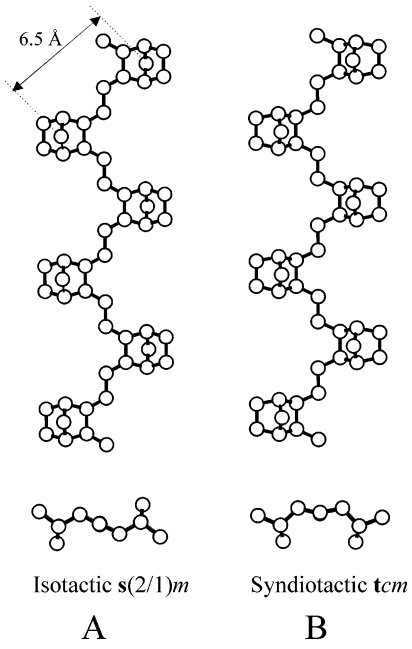

Figure 6. Side views and projections along the chain axes of the models of the chain conformations for isotactic (**s**(2/1)*m* symmetry) (A) and syndiotactic (**t***cm* symmetry) (B) alternating ENC.

sequence of torsion angles (T^- *cis* T^+ T^+ T^+ *cis* T^- T^-)$_n$, according to the **t***cm* symmetry. The chain periodicity calculated for this conformation is 8.84 Å in agreement with the experimental chain axis.

The models of the minimum energy conformations of the isotactic and syndioatctic ENCs are shown in Figure 6.

The conformational energy analysis indicates that both models of the isotactic and syndiotactic chains account for the experimental chain axis periodicity of 8.9 Å, confirming that the crystalline phase in the sample ENC1 may be, in principle, characterized by both isotactic and syndiotactic sequences revealed by the ^{13}C NMR analysis (Figure 1).[21] For these energy minimum conformations, the distance between barycenters of successive norbornene units is 6.4−6.5 Å and the space encumbrance is similar for isotactic and syndiotactic sequences (Figure 6A).

Crystal Structure. As discussed above, since the samples ENC1 and ENC2 present the same X-ray diffraction patterns (Figure 2) and the sample ENC2 is characterized only by isotactic sequences, we can assume that the crystalline phase in these samples is basically characterized by alternating isotactic sequences. For this reason we have studied the crystal structure of alternating ENCs starting with the analysis of possible models of packing of the isotactic ENC chains in the **s**(2/1)*m* conformation of Figure 6A. However, since in the sample ENC1 the crystallization of syndiotactic sequences cannot be excluded we have also analyzed possible models of packing of alternating syndiotactic ENC chains.

It is worth noting that the X-ray diffraction patterns of Figures 2 and 3 present only three reflections (two reflections and a broad halo in the diffraction profile of Figure 2a), indicating the presence of disorder in the structure. For this reason the resolution of the crystal structure cannot be carried out using the traditional methods of crystallography, but a different approach should be used. In particular, the presence of structural

disorder should be considered by analyzing the effect of various kinds of disorder on the X-ray diffraction patterns, and different information, derived, for instance from the geometrical analysis of the chain conformation and calculations of conformational and packing energies, must be used. Moreover, because of the few diffraction data, any model of the crystal structure built up using these information should be not considered as exclusive.

The first information that can be used to obtain models of packing of ENC chains is the great analogy between the X-ray powder diffraction profiles of ENC samples and of low molecular weight crystalline substances characterized by molecules having spherical shape, as adamantane[29a] or norbornane.[29b] The latter structures are characterized by a close packing of the spherical molecules in face-centered cubic lattices, with a positional order of the barycenters of the molecules and orientational disorder of the spherical structural motif. These substances are generally defined "plastic crystals",[30] and present X-ray diffraction patterns characterized by the presence of only a small number of reflections and diffuse scattering, because of the presence of orientational disorder. For instance, the X-ray diffraction profile of norborbane at 40 °C shows only one strong reflection at $2\theta = 17°$ and a second reflection of lower intensity at $2\theta = 20°$,[29b] as in the diffraction profile of ENC of Figure 2a, the only difference is in the much greater sharpness of reflection peaks of norbornane. These two reflections correspond to the 111 and 200 reflections of the face-centered cubic lattice with $a = 8.73$ Å.[29b]

The second important information is given by the X-ray fiber diffraction pattern of Figure 3, which indicates that the most important diffraction feature of the alternating ENCs observed in the powder diffraction profile (Figure 2), that is, the peak of strong intensity at $2\theta = 16.7°$ ($d = 5.31$ Å), corresponds to a first layer line reflection. The second peak of lower intensity at $2\theta = 19.0°$ (Figure 2a) is instead an equatorial reflection (Figure 3 and Table 1). These data confirm the analogy with the structure of plastic crystals. The strong reflection at $2\theta = 16.7°$ is, indeed, mainly due to the atoms of the norbornene rings, whose barycenters are nearly in the same positions for both conformations of isotactic and syndiotactic ENCs chains of Figure 6 and placed at a distance of 6.4−6.5 Å.[22] It could correspond to the diffraction plane containing the atoms of norbornene rings already in the isolated chain. This suggests that the microcrystals of ENC could be characterized by a face-centered nearly cubic mode of packing, typical of plastic crystals. The quite spherical norbornene units could be, indeed, packed in a face-centered crystalline lattice, whose (111) planes containing the norbornene atoms are strongly diffracting, giving the reflection at $2\theta = 16.7°$.[22] In this hypothesis, since the two diffraction peaks observed in the X-ray diffraction profiles at $2\theta = 16.7°$ ($d = 5.31$ Å) and $2\theta = 19.0°$ ($d = 4.67$ Å) correspond to 111 and 200 reflections, norbornene units are placed at nodes of a face-centered nearly cubic lattice with unit cell axes close to 9.3−9.4 Å ($a \approx b \approx c \approx d\sqrt{h^2+k^2+l^2} = 5.31\sqrt{3} = 9.2$ Å from the 111 reflection, and $a \approx b \approx c \approx d\sqrt{h^2+k^2+l^2} = 4.67\sqrt{4} = 9.34$ Å from the 200 reflection, the mean distance between the centers of norbornene units being $(2^{1/2}/2)9.3 \approx 6.57$ Å, as actually occurs (Figure 6).

The X-ray fiber diffraction pattern indicates that the value of the chain axis periodicity $c = 8.9$ Å is only slightly different from that of the supposed a and b axes, indicating a *quasi* tetragonal unit cell with $a = b \approx 9.3-9.4$ Å and $c = 8.9$ Å. The calculated density for the unit cell with $a = b = 9.4$ Å and $c = 8.9$ Å is 1.04 g/cm^3, for two isotactic ENC chains in $\mathbf{s}(2/1)m$ helical conformation included in the unit cell, according to the experimental density of 1.02 g/cm^3, measured by flotation on a ENC1 sample having 20% crystallinity (the density of amorphous ENC, measured by flotation on the ENC1 sample quenched from the melt in liquid N_2, is 1.01 g/cm^3).

This model accounts for the position of the two reflections at $2\theta = 16.7°$ and 19°. However, the X-ray diffraction patterns of Figures 2 and 3 also show diffraction at lower value of 2θ. The diffraction profile of the sample ENC1 present a broad halo of low intensity at values of 2θ in the range 9−10° (Figure 2a), whereas the diffraction profile of the sample ENC2 presents a well-defined peak of low intensity at $2\theta = 9.3°$ ($d = 9.5$ Å, Figure 2b and Table 1). In the proposed model, this peak may be indexed as the 010 (or 100) reflection. The experimental evidence that this reflection may be absent or may transform in a diffuse halo, as for the sample ENC1 (Figure 2a), confirms the presence of disorder and should be explained by the proposed model, as shown in the following. Moreover, the experimental evidence that, in the case of the sample ENC2, the two equatorial reflections are observed at $2\theta = 9.3°$ ($d = 9.5$ Å) and $2\theta = 19°$ ($d = 4.67$ Å) (Figure 2b and Table 1) may possibly indicate that the values of a and b axes are slightly different. These reflections may be, indeed, indexed as 010 and 200 reflections, respectively, of an orthorhombic unit cell with axes $a = 9.3$ Å, $b = 9.5$ Å, and $c = 8.9$ Å, with a similar calculated density of 1.04 g/cm^3. As discussed in the next section, the slightly higher value of the b axis is confirmed by packing energy calculations.

The broadening or the absence of the reflection at $2\theta = 9.3°$ for the sample ENC1 (Figure 2a) indicates that in some samples the disorder is such that the structure can be actually defined by a tetragonal unit cell with $a = b = 9.4$ Å and $c = 8.9$ Å (the diffraction profile of Figure 2a is better accounted for by this tetragonal unit cell, whereas the profile of Figure 2b is accounted for by the orthorhombic unit cell with $a = 9.3$ Å, $b = 9.5$ Å, $c = 8.9$ Å).

These structural data and the analogy with the structure of plastic crystals allow us suggesting that the crystal structure of ENC is defined by the packing of the *quasi*-spherical norbornene units.[22] The barycenters of the norbornene units are arranged on a face-centered crystalline nearly cubic lattice (actually nearly tetragonal or orthorhombic) producing a short-range three-dimensional *positional order*. High amount of disorder in the position of chains is however present in the structure, producing only few diffraction data and, in some samples broadening of some reflections (for instance the reflection at $2\theta = 9.3°$). Only a short-range order in the position of barycenters of norbornene units is maintained, giving the strong 111 reflection.

The structural difference between the samples ENC1 and ENC2 (i.e the absence or the broadening of the reflection at $2\theta = 9.3°$, Figure 2, parts a and b), that can be described by a nearly tetragonal and orthorhombic unit cells, respectively, is probably related to the different microstructures of the samples, which induce different amounts of disorder in the crystals of the two samples. The sample ENC2 is, indeed, much more

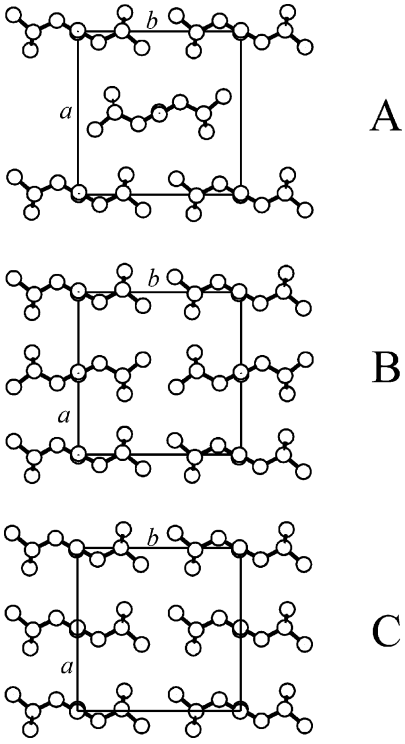

Figure 7. Limit ordered models of packing of isotactic ENC chains in the unit cell with axes $a = b = 9.4$ Å, $c = 8.9$ Å and space group *Pbnm* (A) and in the unit cell with axes $a = 9.3$ Å, $b = 9.5$ Å, $c = 8.9$ Å and space groups *Pcam* (B) and *B*2/*m* (C).

isotactic than the sample ENC1 (Figure 1). The presence of syndiotactic sequences in the sample ENC1, prepared with catalyst **1** of Chart 1, revealed by the ^{13}C NMR spectrum of Figure 1A, induces development of higher degree of disorder, or even different types of disorder.

Models of disorder discussed in the following should be consistent with these hypotheses and able to accounts for all the experimental structural information. We will first describe limit ordered models of packing of isotactic ENC chains and, then, will analyze the effect of introducing different kinds of disorder in the crystals.

The presence of the strong 200 reflection at $2\theta = 19°$ suggests a packing mode along the *a* axis of chains positioned with chain axes at $x = 0$ and $x/a = 0.5$. Three possible limit ordered models for the isotactic ENC are shown in Figure 7. The first model (Figure 7A) is characterized by two isotactic chains in the unit cell with $a = b = 9.4$ Å and $c = 8.9$ Å and chain axes at (0,0,*z*) and (0.5,0.5,*z*). It corresponds to the space group *Pbnm*, with the chain axes coincident with the crystallographic 2-fold axes and the local mirror plane of the **s**(2/1)*m* chains coincident with the mirror plane *m* perpendicular to *c* in the space group. The two helical chains at (0,0,*z*) and (0.5,0.5,*z*) may be distinguished by their shape, depending on the succession *RS* or *SR* of configurations of the two chiral norbornene atoms,[22] the first one having a Z-shape, the second one a S-shape (Figure 7A).[22] In this *Pbnm* model, *bc* layers of chains having alternatively Z-shape and S-shape are piled along *a*, and shifted by 0.5 along *b* (Figure 7A).

The second limit ordered model, shown in Figure 7B, is characterized by two chains having Z- and S-shapes with chain axes at (0,0,*z*) and (0.5,0,*z*) inside the orthorhombic unit cell with $a = 9.3$ Å, $b = 9.5$ Å, $c = 8.9$ Å. In this model *bc* layers of chains having alternatively a Z-shape and S-shape are piled along *a* without shift along *b*, according to the space group *Pcam* (Figure 7B).

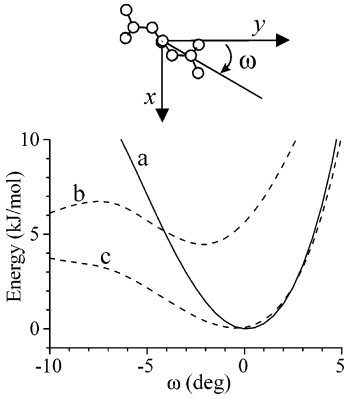

Figure 8. Curves of the packing energy as a function of ω for the limit ordered models of Figure 7A, corresponding to the space group *Pbnm* (a), of Figure 7B, corresponding to the space group *Pcam* (b) and of Figure 7C, corresponding to the space group *B*2/*m* (c). The definition of the angle ω of rotation of the chain around the chain axis is also shown. ω is positive for a clockwise rotation.

The third limit ordered model (Figure 7C) is similar to that of Figure 7B but the chains at (0,0,*z*) and (0.5,0,*z*) have the same Z- or S-shape, according to space group *B*2/*m*. In this model *bc* layers of chains having the same Z-shape or S-shape are piled along *a*, without shift along *b* (Figure 7C).

The models of Figure 7B and C should account for the presence of the 010 reflection at $2\theta = 9.3°$ in the X-ray diffraction profile of the sample ENC2 (Figure 2b), whereas this reflection would be absent for the model of Figure 7A, as observed in the diffraction profile of the sample ENC1 (Figure 2a).

The orientations of the chains around the chain axes in the models of Figure 7 have been found by calculations of the packing energy. Since the atom C7 of the norbornene ring (Figure 4) is in the special position, on the crystallographic mirror plane at $z/c = 0.25$ in the space groups *Pbnm* and *Pcam*, and $z/c = 0$ in the space group *B*2/*m*, the packing energy has been calculated as a function of only one variable, the rotation ω of the chains around their chain axes. Curves of the packing energy as a function of ω, for the limit ordered models in the space group *Pbnm*, *Pcam*, and *B*2/*m* are reported in Figure 8. For the three models minima of the packing energy are obtained for similar values of ω. The packing models of Figure 7 correspond to the minima of the lattice energy of Figure 8.

The packing energy calculations have also indicated that, since from the value of the density two ENC chains must be included in the tetragonal or orthorhombic unit cells, low lattice energies are obtained only when the two chains are positioned with chain axes at (0,0,*z*) and (0.5,*y*,*z*), as in the models of Figure 7. For all these low packing energy models, the 100 reflection, calculated at $2\theta = 9.3-9.4°$, would be absent because of the repetition of chain axes at $x = 0$ and 0.5. Therefore, the diffraction peak observed at $2\theta = 9.3°$ (Figure 2b and Table 1) cannot be interpreted as the first order of the 200 reflection at $2\theta = 19°$ but should be better interpreted as a 010 reflection.

The calculated structure factors for the three limit ordered models of Figure 7 are reported in Tables 3 and 4. Calculations of structure factors have been performed

Table 3. Comparison between Observed Structure Factors (F_o), Evaluated from the Intensities Observed in the X-ray Powder Diffraction Profile of the Sample ENC1 of Figure 2a, and Calculated Structure Factors (F_c) for the Limit Ordered Model of Packing of Isotactic ENC of Figures 7A, in the Space Group *Pbnm*, and for the Limit Disordered Models of Figures 9A (Space Group *Cmcm*), 11A (Space Group *Bbmm*), 11B (Space Group *Acam*), 11C (Space Group *Fmmm*), and 12B (Space Group *I4/mmm*)[a]

						$F_c = (\|F_i\|^2 M_i)^{1/2}$								
$(hkl)_o$	$2\theta_o$ (deg)	$2\theta_c$ (deg)	d_o (Å)	d_c (Å)	F_o	*Pbnm*	*Cmcm*	*Bbmm*	*Acam*	*Fmmm*	$(hkl)_t$	$2\theta_c$ (deg)	d_c (Å)	$F_c = (\|F_i\|^2 M_i)^{1/2}$ *I4/mmm*
010		9.41		9.400		0	0	0	0	0				
110		13.32		6.647		64	64	0	0	0	100	13.32	6.647	0
101		13.70		6.462		40	0	40	0	0				
111	16.7	16.65	5.31	5.325	225	225	225	225	225	225	101	16.65	5.325	235
200	19.0	18.88	4.67	4.700	149	157	157	157	157	157	110	18.88	4.700	118
002	19.8	19.95	4.48	4.450	n.e.[b]	47	47	47	47	47	002	19.95	4.450	47
210		21.13		4.204		41	0	41	0	0				
021		21.38		4.156		27	27	0	0	0	111	21.38	4.156	0
121		23.40		3.801		35	0	35	0	0				
112		24.07		3.698		49	49	0	0	0	102	24.07	3.698	0
022		27.60		3.231		46	46	46	46	46	112	27.60	3.231	34
130		30.06		2.972		67	67	0	0	0	210	30.06	2.972	0
310						71	71	0	0	0				
301		30.24		2.956		55	0	55	0	0				
311		31.74		2.819		31	31	31	31	31	211	31.74	2.819	11
113		33.06		2.709		28	28	28	28	28	103	33.06	2.709	28
222		33.66		2.663		32	32	32	32	32	202	33.66	2.663	32
230		34.40		2.607		77	0	77	0	0				

[a] The Bragg angles ($2\theta_o$) and the Bragg distances (d_o) of reflections observed in the X-ray powder diffraction profile of the sample ENC1 of Figure 2a and those calculated ($2\theta_c$ and d_c) for the orthorhombic unit cell with axes $a = b = 9.4$ Å and $c = 8.9$ Å and the tetragonal unit cell with axes $a = 6.65$ Å and $c = 8.9$ Å are reported. $(hkl)_o$ and $(hkl)_t$ are the indices of the reflections in the orthorhombic and tetragonal unit cells, respectively. Only reflections having calculated structure factors higher than 20 are reported. A complete list of calculated reflections is given as Supporting Information. [b] Since the meridional 002 reflection is observed only in the X-ray fiber diffraction patter of Figure 3, its intensity is not evaluated (n.e.).

Table 4. Comparison between Observed Structure Factors (F_o), Evaluated from the Intensities Observed in the X-ray Powder Diffraction Profile of the Sample ENC2 of Figure 2b, and Calculated Structure Factors (F_c) for the Limit Ordered Models of Packing of Isotactic ENC of Figures 7B,C, in the Space Groups *Pcam* and *B2/m*, Respectively, and for the Limit Disordered Model of Figures 9B in the Space Group *Bmcm*[a]

						$F_c = (\|F_i\|^2 M_i)^{1/2}$		
$(hkl)_o$	$2\theta_o$ (deg)	$2\theta_c$ (deg)	d_o (Å)	d_c (Å)	F_o	*Pcam*	*B2/m*	*Bmcm*
010	9.3	9.31	9.5	9.500	60	40	41	41
101		13.77		6.430		0	35	0
111	16.7	16.65	5.31	5.325	225	226	216	225
200	19.0	19.09	4.67	4.650	147	163	158	158
002	19.8	19.95	4.48	4.450	n.e.[b]	47	47	48
210		21.27		4.176		66	35	71
201		21.56		4.121		44	0	0
012		22.06		4.030		41	42	41
121		23.28		3.821		23	14	23
022		27.46		3.248		47	46	46
030		28.18		3.167		49	53	53
221		28.68		3.113		53	0	0
212		29.33		3.045		31	29	28
130		29.80		2.998		56	0	0
310		30.33		2.947		34	0	0
301		30.54		2.928		0	54	0
311		31.99		2.798		38	28	33
113		33.07		2.709		30	20	29
222		33.66		2.662		26	40	30
230		34.26		2.617		44	32	46

[a] The Bragg angles ($2\theta_o$) and the Bragg distances (d_o) of reflections observed in the X-ray powder diffraction profile of the sample ENC2 of Figure 2b and those calculated ($2\theta_c$ and d_c) for the orthorhombic unit cell with axes $a = 9.3$ Å, $b = 9.5$ Å and $c = 8.9$ Å are reported. $(hkl)_o$ are the indices of the reflections in the orthorhombic unit cell. Only reflections having calculated structure factors higher than 20 are reported. A complete list of calculated reflections is reported on the web as supporting materials. [b] Since the meridional 002 reflection is observed only in the X-ray fiber diffraction patter of Figure 3, its intensity is not evaluated (n.e.).

using a constant value of the thermal parameter $B = 8$ Å^2, typical of polymer crystals. The value of B has not been optimized because of the few available diffraction data, and it produces reasonable mean-square root displacement of atoms due to thermal disorder. Only the models *Pcam* and *B2/m* (Figure 7, parts B and C, respectively) account for the presence of the 010 reflection at $2\theta = 9.3°$ in the X-ray diffraction pattern of Figure 2b (Table 4). The presence of a diffuse halo in the 2θ range 8−10° in the pattern of Figure 2a, instead of the sharp reflection, indicates that disorder in the shift along *b* of *bc* layers of chains is present (*b* shift disorder). The crystalline domains are probably characterized by disordered packing modes intermediate between the limit ordered models of Figure 7. Different crystalline domains, characterized by both packing modes of Figure 7, diffracting coherently, may be also present.

As shown in Tables 3 and 4, the calculated structure factors are not in agreement with the experimental intensities because of the presence of many reflections with strong or medium calculated intensities, which are not observed in the experimental patterns of Figures 2 and 3 (for instance the 110, 101, 210, 112, and 130 reflections at $2\theta = 13.3$, 13.7, 21.1, 24.1, and 30.1°, respectively, for the space group *Pbnm*, or the 210, 201, 012, 022, 030, and 221 reflections at $2\theta = 21.3$, 21.6, 22.1, 27.5, 28.2, and 28.7°, respectively, for the space group *Pcam*, or the 101, 210, 012, 022, and 030 reflections at $2\theta = 13.8$, 21.3, 22.1, 27.5, and 28.2°, respectively, for the space group *B2/m*). This indicates that disorder is present in the structure. As discussed above, a possible disorder may be due to shifts along *b* of successive *bc* layers of chains piled along *a* (*b* shift disorder), producing packing modes intermediate between those of the limit ordered models of Figure 7. We first will discuss different kinds of disorder probably present in the models of Figure 7, and then we will consider the *b* shift disorder.

A first kind of possible disorder present in the structures of Figure 7 may be related to the statistical substitution of chains having S-shape and Z-shape in

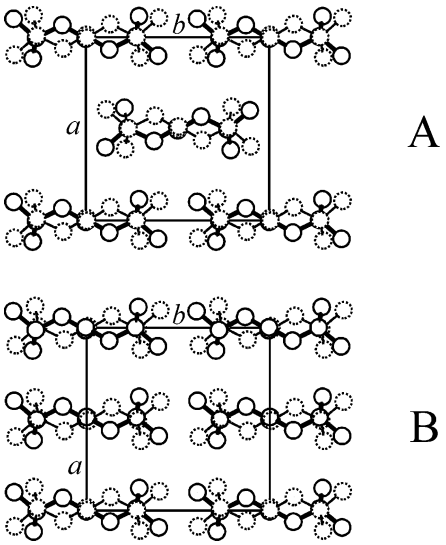

Figure 9. Limit disordered models of packing of isotactic ENC chains in the orthorhombic unit cell with axes $a = b = 9.4$ Å and $c = 8.9$ Å, corresponding to the statistical space group *Cmcm* (A), and in the unit cell with $a = 9.3$ Å, $b = 9.5$ Å, and $c = 8.9$ Å and statistical space group *Bmcm* (B). In both models, chains having S- and Z-shapes are present in each site of the lattice with the same probability.

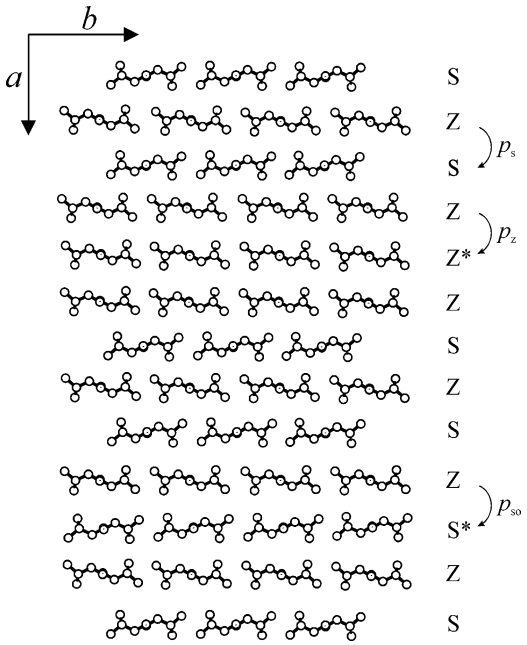

Figure 10. Model of packing of isotactic ENC chains showing disorder in the succession along *a* of *bc* layers of chains having S- and Z-shapes. A *bc* layer of chains having Z-shape is succeeded along *a* by a *bc* layer of chains having S-shape and shifted by *b*/2 along *b* (like in the model of Figure 7A), with probability p_s, or by a *bc* layer of chains having the same Z-shape without shift along *b* (like in the model of Figure 7C), with probability p_z, or by a *bc* layer of chains having S-shape without shift along *b* (like in the model of Figure 7B), with probability p_{so}. In a structure characterized prevailingly by the model of Figure 7A, the Z* and S* layers indicate defective *bc* layers of chains.

each site of the lattice. This statistical substitution is feasible because two chains with S- and Z-shapes have the norbornene rings approximately in the same positions. The presence of this kind of disorder (S−Z disorder) produces a statistical centering of the *ab* or *ac* faces of the unit cells in the models *Pbnm* and *Pcam* of Figure 7, parts A and B, respectively; the limit disordered models, shown in Figure 9, parts A and B, may be described by the statistical space groups *Cmcm* and *Bmcm*, respectively. The calculated structure factors for the two limit disordered models of Figure 9 are also reported in Tables 3 and 4. It is apparent that, for both models, the agreement between calculated and observed intensities is improved by the presence of the S−Z disorder. In fact, for the models *Cmcm* and *Bmcm* (Figure 9A and B), the statistical centering of the *ab* or *ac* face of the unit cell, respectively, and the statistical presence of the glide plane *c* perpendicular to the *b* axis, causes the extinction of the *hkl* reflections with $h + k$ or $h + l$ odd and of the *h*0*l* reflections with *l* odd. For instance, the 101 and 210 reflections, calculated with strong intensities for the limit ordered model *Pbnm*, but absent in the experimental X-ray diffraction patterns, are annulled for the corresponding statistical disordered model *Cmcm* (Table 3). Analogously, the 201 and 221 reflections, calculated for the ordered model *Pcam*, and the 101 and 301 reflections, calculated for the ordered model *B*2/*m*, are absent for the disordered model *Bmcm* (Table 4), according to the experimental patterns. However, the presence of this kind of S−Z shape disorder is not sufficient to account for the experimental X-ray diffraction patters, because in both *Cmcm* and *Bmcm* models of Figure 9, some not observed reflections are still calculated with strong or medium intensities, as for instance, 110, 112, 022, and 130 reflections for the model *Cmcm*, and 210, 012, 022, and 030 reflections for the model *Bmcm* (Tables 3 and 4). This indicates that other kinds of disorder are present in the structure along with the S−Z shape disorder.

As discussed above, other kinds of disorder correspond to the disorder in the positioning along *b* of *bc* layers of chains (*b*-shift disorder). This disorder produces packing modes intermediate between limit ordered models of Figure 7A (space group *Pbnm*), 7B (space group *Pcam*) and 7C (space group *B*2/*m*). Disorder may, indeed, arise from the statistical succession along *a* of *bc* layers of chains having opposite shape (S- and Z-shapes) and shifted along *b* by *b*/2, like in the ordered model of Figure 7A (space group *Pbnm*), or without shift, like in the model of Figure 7B (space group *Pcam*), or having the same shape without shift along *b*, like in the model of Figure 7C (space group *B*2/*m*). A structural model containing this kind of disorder is shown in Figure 10, as an example. A *bc* layer of chains having Z-shape is succeeded along *a* by a *bc* layer of chains having S-shape shifted by *b*/2 along *b* with probability p_s, or without shift with probability p_{so}, or by a *bc* layer having the same Z-shape without shift along *b* with probability p_z.

Limit disordered models characterized by statistical disorder of the kind described in Figure 10, may be described by the statistical space groups *Bbmm* and *Acam*. The model *Bbmm*, shown in Figure 11A, is characterized by a statistical succession along *a* of *bc* layers of chains having opposite shape (S- and Z-shapes) and shifted along *b* by *b*/2, like in the ordered model of Figure 7A, or having the same shape without shift along *b*, like in the model of Figure 7C. The presence of this kind of disorder seems reasonable because the statistical substitution of a Z-chain with a S-chain shifted along *b* by *b*/2, does not change significantly the positions of the norbornene rings inside each *bc* layer of chains, whereas only the atoms of the ethylene units are statistically distributed in the positions (0,0,*z*), (0,0.5,*z*), (0.5,0,*z*), and (0.5,0.5,*z*) of the unit cell (Figure 11A).

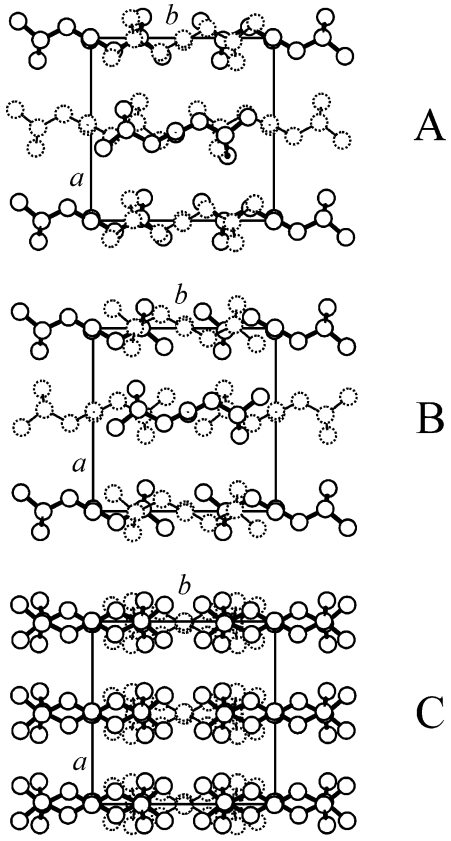

Figure 11. Limit disordered models of packing corresponding to space groups *Bbmm* (A), *Acam* (B), and *Fmmm* (C). The model *Bbmm* is characterized by a statistical succession along *a* of *bc* layers of chains having the same shape, without shift along *b*, or opposite shape with *b*/2 shift along *b* (A). The model *Acam* is characterized by a succession along *a* of *bc* layers of chains having opposite shape, each layer statistically shifted along *b* by 0 or *b*/2 (B). The model *Fmmm* is characterized by statistical S−Z shape disorder and *b* shift disorder; chains having S- and Z-shapes may be present in each site of the lattice with the same probability, and *bc* layers of chains, composed of S and Z chains, succeed along *a* statistically shifted along *b* by 0 or *b*/2.

The model *Acam*, shown in Figure 11B, is characterized by a succession of Z and S-layers along *a*, each layer statistically shifted along *b* by 0 or *b*/2. Also with this kind of disorder, the statistical substitution of a Z-chain with a Z-chain shifted along *b* by *b*/2, does not change significantly the positions of the norbornene rings inside each *bc* layer of chains, whereas only the atoms of the ethylene units are statistically distributed in the positions (0,0,*z*), (0,0.5,*z*), (0.5,0,*z*), and (0.5,0.5,*z*) of the unit cell (Figure 11B). Each *bc* layer of chains is composed of all S- or Z-chains.

The calculated structure factors for the limit disordered models of Figure 11 are reported in Table 3. It is apparent that in the case of the model *Bbmm* (Figure 11A), the presence of disorder produces an improvement of the agreement with respect of the limit ordered models of Figure 7. In fact the not observed 110, 201, 012, 112, and 130 reflections, calculated with strong or medium intensities in the ordered models of Figure 7, parts A or B, are absent for the model *Bbmm* of Figure 11A (Table 3). Also in this case, however, other not observed reflections, i.e., 101, 210, and 121 reflections, are still calculated with strong intensities. In the case of the disordered model *Acam* of Figure 11B, most of the not-observed reflections, i.e., 110, 101, 210, 201, 012, 112, and 130 reflections, calculated with strong or medium intensities for the ordered models of Figure 7, are absent (Table 3) and only the 111, 200, and 002 reflections are calculated with strong intensities according to the experimental X-ray diffraction patterns.

These calculations indicate that the disordered model of Figure 11B (space group *Acam*) shows the best agreement between calculated and observed X-ray intensities. However, it is reasonable that the different kinds of disorder here considered may be simultaneously present in the structure. In fact, in the models of Figure 11, parts A (*Bbmm*) and B (*Acam*), *bc* layers of chains, composed of chains having a defined shape and statistically positioned with chain axes at (*x*,0,*z*) or (*x*,0.5,*z*), succeed along *a*, and the chains facing each other along *a* have the same shape (Figure 11A, space group *Bbmm*) or opposite shape (Figure 11B, space group *Acam*). In these models the S−Z shape disorder, like in the models of Figure 9, may be present as well; i.e., in each site of the lattice, chains having S-shape or Z-shape may be present with the same probability. In other words, *bc* layers of chains, statistically composed of S- and Z-chains, succeed along *a* with *b*-shift disorder, i.e., each layer statistically shifted along *b* by 0 or *b*/2. A limit disordered model containing the S−Z-shape disorder and the *b* shift disorder is shown in Figure 11C. This statistical disorder produces a statistical centering of the *ab*, *ac*, and *bc* faces of the unit cell, and the model can be described by the statistical space group *Fmmm*. The calculated structure factors for the limit disordered model of Figure 11C are also reported in Table 3. It is apparent that when the different kinds of disorder are simultaneously present a fairly good agreement between calculated and experimental X-ray diffraction intensities is obtained.

It is worth noting that in all the presented structure models the relative arrangements of chains around the 2-fold axes define *bc* layers of chains piled along the *a* axis (Figures 7 and 11). Since the *a* and *b* axes of the unit cell have nearly equal length, the chains may be rotated around the chain axes by 90°, defining *ac* layers of chains, perpendicular to the *bc* layers, piled along *b*. This suggests that another kind of disorder may be present in the structure. The disorder corresponds to the presence of domains characterized by *bc* layers of chains piled along *a*, stacked along *b* with *ac* layers of chains, perpendicular to the *bc* layers, as shown in Figure 12A. In each *bc* or *ac* layer the statistical S−Z disorder of the chains and the *b*-shift disorder (*a*-shift for the *ac* layers) are present. This disorder may be described by the limit disordered model reported in Figure 12B. This model is characterized by the statistical presence of *bc* and *ac* layers of chains, perpendicular to each other, having the atoms of the norbornene rings almost in the same positions. The atoms of the ethylene units are instead statistically positioned between all the norbornene rings. Therefore, the model of Figure 12B keeps the same structural features of the disordered models described above (Figure 11), the positions of the atoms of the norbornene units being nearly the same as in the models of Figure 11. The atoms of the ethylene units are instead statistically positioned along *b* at 0, *b*/4, *b*/2, and $^3/_4b$ and along *a* at 0, *a*/4, *a*/2, and $^3/_4a$ (Figure 12B), and the layers of chains turn out to be related by 4-fold rotation axes of symmetry. The statistical presence of perpendicular layers of chains related by a 4-fold rotation symmetry, produces, in the

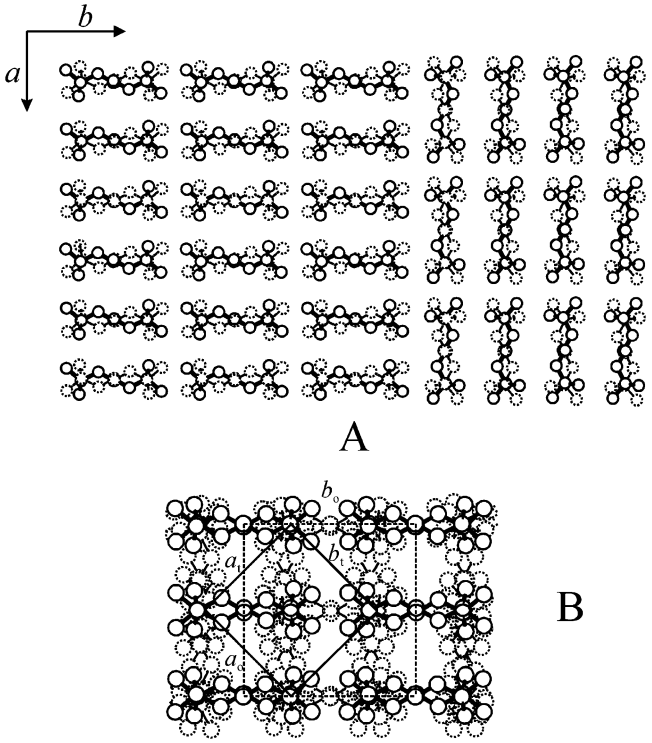

Figure 12. (A) Disordered model of packing of isotactic ENC chains characterized by the presence of domains containing *bc* layers of chains piled along *a*, stacked along *b* with *ac* layers of chains piled along *b*. The chains in the *ac* layers are rotated around the chain axes by 90° with respect to the chains in the *bc* layers. Each domain (*bc* layers piled along *a*, and *ac* layers piled along *b*) present the statistical S−Z shape disorder. (B) Limit disordered model characterized by the statistical presence of *bc* layers and *ac* layers of chains perpendicular to each other in the tetragonal unit cell, according to the statistical tetragonal space group *I*4/*mmm*. The statistical S−Z shape disorder and statistical shifts of *bc* layers along *b* by 0 or *b*/2, and *ac* layers along *a* by 0 and *a*/2 are also present. The tetragonal unit cell with axes $a = b = 6.65$ Å and $c = 8.9$ Å is shown as continuous lines, whereas the orthorhombic unit cell with axes $a_0 = b_0 = 9.4$ Å is shown as dotted lines.

model of Figure 12B, a statistical tetragonal symmetry of the lattice. The limit disordered model of Figure 12B may be, indeed, described with a smaller tetragonal unit cell with axes $a = b = 6.65$ Å and $c = 8.9$ Å and by the statistical tetragonal space group *I*4/*mmm*. This model presents all the different kinds of disorder described above.

The calculated structure factors for the limit disordered model of Figure 12B (space group *I*4/*mmm*), are reported in Table 3. It is apparent that only the reflections at $2\theta = 16.7$ and 19.0°, indexed as 101 and 110 reflections for the tetragonal unit cell, and the 002 reflection are calculated with strong intensities, according to the experimental X-ray diffraction patterns, and a fairly good agreement between calculated and experimental intensities has been obtained. A direct comparison between the calculated X-ray diffraction profiles for the disordered models of Figure 11C (space group *Fmmm*) and 12B (space group *I*4/*mmm*) and the experimental profile of the sample ENC1 is shown in Figure 13A. A good agreement for both disordered models is apparent. Similar comparison between the calculated diffraction profile for the model of Figure 9B (space group *Bmcm*) and the experimental X-ray diffraction profile of sample ENC2 is shown in Figure 13B.

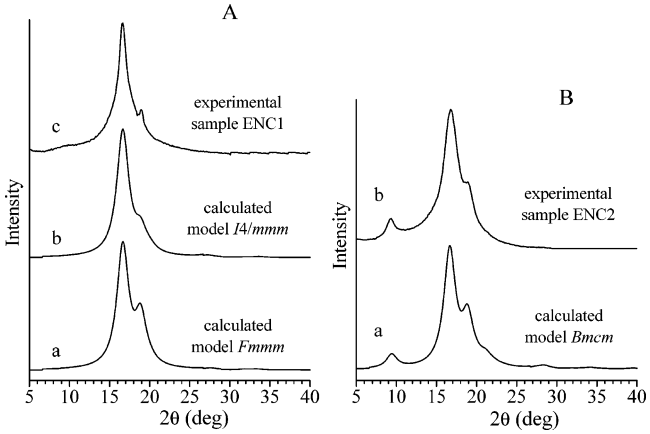

Figure 13. (A) Comparison between calculated X-ray diffraction profiles for the limit disordered models *Fmmm* of Figure 11C (a) and *I*4/*mmm* of Figure 12B (b) and the experimental X-ray powder diffraction profile of the sample ENC1 (c). (B) Comparison between the calculated X-ray diffraction profile for the limit disordered model *Bmcm* of Figure 9B (a) and the experimental X-ray powder diffraction profile of the sample ENC2 (b).

It is apparent the disordered models of Figures 11C and 12B account for the diffraction profile of the sample ENC1, whereas the orthorhombic model of Figure 9B accounts for the diffraction profile of sample ENC2. These results indicate that the crystal structure of ENC is characterized by many different kinds of structural disorder, which may be simultaneously present in the structure. Some structural features are however well-defined; for instance, an order in the average positioning of the barycenters of norbornene rings is present in the structure. These features can be described by the ideal limit ordered models of Figure 7. The few reflections present in the X-ray diffraction patterns allows one to assume that the order rapidly fades away with increasing distance between the norbornene units. Disorder in the positioning of the carbon atoms of the ethylene units is always present. The real crystalline modifications are probably intermediate between the limit ordered models of Figure 7 and the limit disordered models described in Figures 9, 11, and 12B. The amount and the kind of disorder depend, probably, on the microstructure of the chains and on the condition of crystallization. For instance, the sample ENC2 is probably crystallized in a modification characterized by a packing of the chains closer to the model of Figure 9B (*Bmcm*), because of the presence in the X-ray diffraction profile of the 010 reflection at $2\theta = 9.3°$ (Figure 13B). The sample ENC1 is, instead, crystallized in a modification characterized by a large amount of *b*-shift disorder, closer to the models of Figures 11C (*Fmmm*) and 12B (*I*4/*mmm*), since the 010 reflection appears as a broad halo in the X-ray diffraction profile (Figure 13A).

The tetragonal model of Figure 12B could be, therefore, representative of the small "crystals" constituting the crystalline fringed micelle bundles in sample ENC1. The crystals are characterized by positional order of the barycenters of the norbornene units and orientational disorder, due to the fact that the chain may connect with equal probability a given norbornene unit with any of its next neighbors. The ethylene units, connecting the norbornene units, may, indeed, assume different positions along *a* and *b* axes, producing *orientational* disorder of the chains as well as of the *quasi*-spherical norbornene units, whose barycenters remain organized

on the face-centered lattice, producing the strong reflection at $2\theta = 16.7°$ on the first layer line. This kind of disorder is consistent with the observation that the X-ray fiber diffraction pattern of Figure 3 presents a diffuse, continuous background scattering subtending the Bragg reflections. The main effect of the orientational disorder in the model of Figure 12, indeed, is to smear out the electron density of norbornene ball-like units on the surfaces of spheres of average radius equal to ~4.5 Å, that is the square-root of the mean square radius of a norbornane molecule. It may be shown that the diffuse scattering associated with this kind of disorder is zero at $2\theta = 0$ and increases smoothly with increasing 2θ up to a constant value.

Although this model of disorder accounts for the experimental diffraction patterns, the proposed model of packing should not be considered as exclusive because of the few available diffraction data. Different models of packing able to explain the positions of the three reflections present in the diffraction profiles of Figure 2 could be easily found. However, less simple is finding models of disorder able to keep in the diffraction pattern only the three reflections at $2\theta = 9.3$, 16.7 and 19°, while destroying diffraction on other crystallographic planes. Our model, even though not exclusive, gives a reasonable explanation of the most important features of the organization of the ENC polymer chains. The analogy with the structure of plastic crystals and the conformational and packing energy calculations support the proposed model.

As discussed above, the proposed model of the crystal structure of ENC is based on the assumption of a regular diisotactic configuration of the chains of the alternating copolymer. However, since the NMR analysis of the sample ENC1 has shown the presence of a not negligible fraction of syndiotactic EN sequences,[21] we have also considered the possible crystallization of syndiotactic sequences, eventually compatible with the crystallization of isotactic ones. Possible ideal models of packing of syndiotactic ENC chains have been analyzed and the corresponding calculated X-ray diffraction profile compared with the experimental one.

As shown in previous sections, the conformations of isotactic and syndiotactic chains are very similar (Figure 6), despite the different configurations and the different symmetries relating successive monomeric units along the chains (helical **s**(2/1)*m* and **t***cm* for isotactic and syndiotactic chains, respectively). Both are nearly extended and present similar values of the chain periodicity (8.9 Å) and similar outside envelope, which is defined mainly by the position of the norbornene rings (Figure 6). This suggests that a possible ideal model of packing of alternating syndiotactic ENC chains should be very similar to those proposed for the isotactic chains.

A limit ordered model of packing of syndioatctic ENC chains, similar to that of Figure 7A for the isotactic chains, is shown in Figure 14A. Syndiotactic chains in the extended conformation with **t***cm* symmetry are packed in the same unit cell with axes $a = b = 9.4$ Å, $c = 8.9$ Å, and chain axes positioned at (0,0,*z*) and (0.5,0.5,*z*), according to the space group *C*2*cm*. The same kinds of disorder as in the case of the models of packing of isotactic chains (Figures 9, 10 and 11), for instance disorder in the shift along *b* of *bc* layers of chains piled along *a*, may be present. A limit disordered model, characterized by the statistical succession along *a* of *bc* layers of chains, shifted along *b* by *b*/2, or without shift,

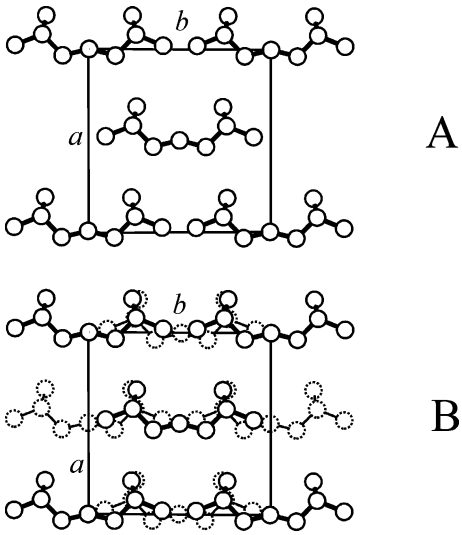

Figure 14. Limit ordered model of packing of syndiotactic ENC chains in the **t***cm* conformation in the orthorhombic unit cell with axes $a = b = 9.4$ Å and $c = 8.9$ Å and space group *C*2*cm* (A). Limit disordered model characterized by a succession along *a* of *bc* layers of chains statistically shifted along *b* by 0 or *b*/2, according to the statistical space group *F*2*mm* (B).

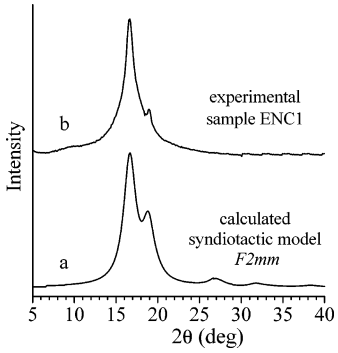

Figure 15. Comparison between the calculated X-ray diffraction profiles for the limit disordered model of packing of syndiotactic ENC chains of Figure 14B, space group *F*2*mm* (a), and the experimental X-ray powder diffraction profile of the sample ENC1 (b).

may be described by the statistical space group *F*2*mm* and is shown in Figure 14B.

A comparison between the experimental and calculated X-ray diffraction profiles for the disordered model of Figure 14B is shown in Figure 15. It is apparent that for the limit disordered model a good agreement is obtained, even though the intensities of reflections at $2\theta = 19$ and 27° are calculated too high, indicating that higher amount of disorder should be present, as in the isotactic model structures of Figures 11 and 12.

These results indicate that the possible crystallization of syndiotactic sequences, present in the sample ENC1 (revealed by the NMR spectrum of Figure 1A), is compatible with the observed crystallinity. In ENC samples, chains in prevailing isotactic configuration crystallize in disordered modifications characterized by packing modes shown in Figures 9B, 11, and 12B; relatively short syndiotactic sequences may be present as defects and may cocrystallize with the longer isotactic ones. The partial three-dimensional order, guided by the ordered positioning of the ball-like norbornene units, producing the observed crystallinity, is obtained even though the polymers are configurationally disordered,

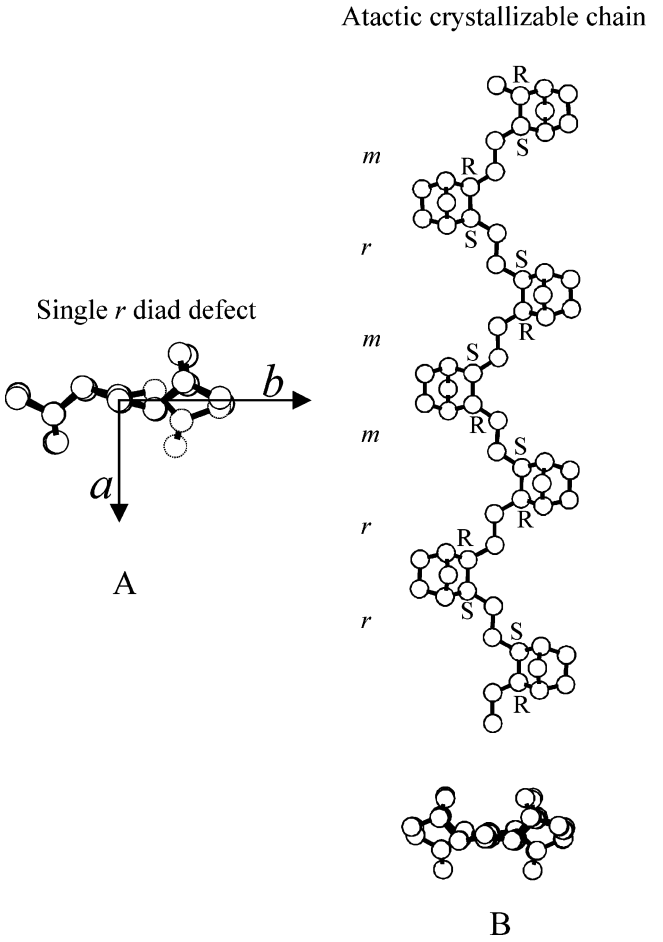

Figure 16. (A) Projection in the *ab* plane of an isotactic ENC chain containing a single defect of stereoregularity corresponding to a syndiotactic *r* diad (dotted lines). (B) Side view and projection in the *ab* plane of an atactic crystallizable ENC chain charactized by a statistical succession of *m* and *r* diads. The configurations *R* and *S* of the chiral atoms of norbornene units are indicated.

provided that they have a regular alternation of the comonomeric units.

It is worth noting that the main difference between syndiotactic and isotactic sequences in ENC chains is the relative position of the norbornene rings (Figure 6). As shown in Figure 16A, in an isotactic chain containing a single configurational defect (a syndiotactic *r* diad) the atoms of consecutive norbornene rings in a syndiotactic sequence project on the *ab* plane along the same *a* axis direction, whereas they project along opposite *a* direction in the regular isotactic sequences. An atactic ENC chain, charactized by a statistical succession of isotactic *m* and syndiotactic *r* diads, is shown in Figure 16B. It is apparent that atactic chains may be still straight and maintain the same shape as in regular isotactic and syndiotactic chains of Figure 6. Therefore, atactic chains, or chains containing blocks of short isotactic and syndiotactic sequences, may crystallize. Moreover, the projection in the *ab* plane of the atactic chain of Figure 16B clearly shows that the presence of configurational defects in an isotactic chains (*r* diads or longer syndiotactic sequences), or of statistical disorder in the succession of configurations, produces the same effects as that produced by the statistical replacement of isotactic chains having S- and Z-shapes (Figure 9). This suggests that the presence of configurational defects may give a contribution to the development of the S−Z shape disorder and the *b*-shift disorder found in the crystal structure of ENC (Figures 9B, 11, and 12).

Conclusions

A model for the crystal structure of alternating ethylene−norbornene copolymer is proposed. Oriented fibers of ENCs have been obtained and the corresponding X-ray fiber diffraction pattern has been reported for the first time. A value of the chain axis periodicity of 8.9 Å has been evaluated. Geometrical and conformational energy analyses have shown that isotactic ENC chains assume 2-fold helical conformation with **s**(2/1)-*m* symmetry, whereas syndiotactic chains assume t*cm* conformation. Both conformations account for the experimental chain axis periodicity of 8.9 Å.

Samples of ENCs prepared with different catalysts present different microstructures, characterized by isotactic and syndiotactic sequences (sample ENC1) or prevailing isotactic configuration (sample ENC2). The samples show similar X-ray diffraction patterns, which are accounted for by a model of packing of isotactic ENC chains in orthorhombic unit cells with $a = b = 9.4$ Å and $c = 8.9$ Å, or $a = 9.3$ Å, $b = 9.5$ Å, and $c = 8.9$ Å.

The crystal structure is mainly defined by the packing of the *quasi*-spherical norbornene units. The barycenters of the norbornene units are arranged on a face-centered crystalline lattice, producing a short-range three-dimensional *positional order*. The few reflections present in the X-ray diffraction patterns allows assuming that the order rapidly fades away with increasing the distance between the norbornene units.

Different kinds of structural disorder are present in the structure. A short-range order in the average positioning of the norbornene rings is maintained, while disorder in the positioning of the carbon atoms of the ethylene units is present. The ethylene units may assume different positions along *a* and *b* axes of the unit cell and connect with equal probability a given norbornene unit with any of its next neighbors, producing *orientational disorder* of the polymer chains as well as of the spherical norbornene units.[22]

This structure represents a first example of polymeric crystals characterized by positional order and orientational disorder of the structural motif, as in "plastic" crystals of molecules having a spherical shape, as for instance adamantane or norbornane.[22]

The amount and the kind of disorder depend, probably, on the microstructure of the chains and on the condition of crystallization. For instance, the more isotactic sample ENC2 is basically crystallized in a disordered modification characterized by a packing of the chains close to the model described by the statistical space group *Bmcm* of Figure 9B. The sample ENC1, containing isotactic and syndiotactic sequences, is crystallized instead mainly in a disordered modification characterized by a large amount of *b*-shift disorder, closer to the models *Fmmm* or *I*4/*mmm* of Figures 11C and 12B, respectively.

The limit disordered tetragonal model of Figure 12B, containing all the considered kinds of statistical disorder may be described by the tetragonal unit cell with axes $a = b = 6.65$ Å and $c = 8.9$ Å and the space group *I*4/*mmm*. According to this model, representative of the small "crystals" constituting the crystalline fringed micelle bundles in the sample ENC1, the crystals are characterized by positional order of the barycenters of the norbornene units and orientational disorder, due to

the fact that the chain may connect with equal probability a given norbornene unit with any of its next neighbors. Although this model of disorder accounts for the experimental diffraction patterns, the proposed model of packing should not be considered as exclusive because of the few available diffraction data.

Defects of stereoregularity, characterized by *r* diads or longer syndioatctic sequences, are easily tolerated in the structure of the prevailing isotactic chains. The cocrystallization of syndiotactic sequences, eventually present, is compatible with the observed crystallinity. The partial threedimensional order, guided by the ordered positioning of the ball-like norbornene units, producing the observed crystallinity, is obtained even though the polymers are configurationally disordered, provided that they have a regular alternation of the comonomeric units.

The structural features of ENCs recall not only the packing of plastic crystals but also that of "ionenes",[31] polymeric ionic salts of general formula $-[-(CH_2)_m-NR_2-]_nqn$X where the cationic NR_2^+ and monovalent ($q = 1$) or bivalent ($q = 0.5$) anionic X species are regularly spaced along the main chain. Ionenes may crystallize in pseudocubic tetragonal lattices with ionic sites X and $-NR_2-$ arranged in a regular face-centered lattice.[31] A long-range crystalline order is produced because of the strong electrostatic interactions between cationic NR_2^+ and anionic X groups. However, the position of the polymer chain connecting the ammonium groups is disordered, since the chain may connect with equal probability a given N carbon with its eight next neighbors. As in ENC, the pseudocubic structure is defined by the packing of spherical motifs, while the arrangement of the polymer chains is disordered.

Acknowledgment. Financial supports from the "Ministero dell'Istruzione, Università e Ricerca Scientifica" (PRIN 2002 and Cluster C26 projects) are gratefully acknowledged.

Supporting Information Available: Tables showing a comparison between observed structure factors evaluated from the intensities observed in the X-ray powder diffraction profiles of ENC samples and calculated structure factors for the limit ordered and limit disordered models of packing of isotactic and syndiotactic ENC and fractional coordinates of the asymmetric units in the proposed models of the crystal structure of ENC. This material is available free of charge via the Internet at http://pubs.acs.org.

References and Notes

(1) Kaminsky, W. *Macromol. Chem. Phys.* **1996**, *197*, 3907.
(2) Kaminsky, W.; Noll, A. *Polym. Bull. (Berlin)* **1993**, *31*, 175.
(3) Kaminsky, W.; Bark, A.; Steiger, R. *J. Mol. Catal.* **1992**, *72*, 109.
(4) Kaminsky, W.; Bark, A.; Arndt, M. *Makromol. Chem. Macromol. Symp.* **1991**, *47*, 83.
(5) Haselwander, T. F. A.; Heitz, W.; Krügel, S. A.; Wendorff, J. H.; *Macromol. Chem. Phys.* **1996**, *197*, 3435.
(6) Cherdron, H.; Brekner, M.-J.; Osan, F. *Angew. Makromol. Chem.* **1994**, *223*, 121.
(7) Arndt, M.; Kaminsky, W. *Macromol. Symp.* **1995**, *97*, 225.
(8) Ruchatz, D.; Fink, G. *Macromolecules* **1998**, *31*, 4669.
(9) Ruchatz, D.; Fink, G. *Macromolecules* **1998**, *31*, 4674.
(10) Ruchatz, D.; Fink, G. *Macromolecules* **1998**, *31*, 4681.
(11) Ruchatz, D.; Fink, G. *Macromolecules* **1998**, *31*, 4684.
(12) Brekner, M.-J.; Osan, F.; Rohrmann, J.; Antberg, M. (Hoechst AG) U.S. Patent 5,324,801, 1994.
(13) Lang, H. T.; Osan, F.; Wehrmeister, T. *Polym. Mater. Sci. Eng.* **1997**, *76*, 22. Kaminsky, W.; Arndt-Rosenau, M. *Metallocene-based Polyolefins*; Scheirs, J., Kaminsky, W., Eds.; John Wiley: New York, 2000.
(14) Tritto, I.; Boggioni, L.; Sacchi, M. C.; Locatelli, P. *J. Mol. Catal. A: Chem.* **1998**, *133*, 139. Tritto, I.; Boggioni, L.; Sacchi, M. C.; Locatelli, P.; Ferro, D. R.; Provasoli, A. *Macromol. Rapid Commun.* **1999**, *20*, 279. Provasoli, A.; Ferro, D. R.; Boggioni, L.; Tritto, I. *Macromolecules* **1999**, *32*, 6697. Tritto, I.; Marestin, C.; Boggioni, L.; Sacchi, M. C.; Brintzinger, H. H.; Ferro, D. R. *Macromolecules* **2001**, *34*, 5770.
(15) Arndt, M.; Beulich, I. *Macromol. Chem. Phys.* **1998**, *199*, 1221. Arndt, M.; Beulich, I. *Macromolecules* **1999**, *32*, 7335.
(16) Arndt, M.; Engehausen, R.; Kaminsky, W.; Zoumis, K. *J. Mol. Catal. A: Chem.* **1995**, *101*, 171.
(17) Brintzinger, H. H.; Fischer, D.; Mulhaupt, R.; Rieger, B.; Waymouth, R. M. *Angew. Chem.* **1995**, *107*, 1255.
(18) Harringhton, B. A.; Crowther, D. J. *J. Mol. Catal. A: Chem.* **1998**, *128*, 79.
(19) McKnight, A. L.; Waymouth, R. M. *Macromolecules* **1999**, *32*, 2816.
(20) Grassi, A.; Maffei, G.; Milione, S.; Jordan, R. F. *Macromol. Chem. Phys.* **2001**, *202*, 1239.
(21) Altamura, P.; Grassi, A. *Macromolecules* **2001**, *34*, 9197.
(22) De Rosa, C.; Corradini, P.; Buono, A.; Auriemma, F.; Grassi, A.; Altamura, P. *Macromolecules* **2003**, *36*, 3789.
(23) Cromer, D. T.; Mann, J. B. *Acta Crystallogr.* **1968**, *A24*, 321.
(24) Allinger, N. L.; Yuh, Y. H. *QCPE* **1980**, *12*, 395.
(25) Yoon, D Y.; Sundarajan, P. R.; Flory, P. J. *Macromolecules* **1975**, *8*, 765.
(26) Corradini, P.; Petraccone, V.; Pirozzi, B. *Eur. Polym. J.* **1983**, *19*, 299.
(27) Corradini, P. In *The Stereochemistry of Macromolecules*; Ketley, A. D., Ed.; Marcel Dekker Inc.: New York, 1968; Vol. 3.
(28) Ahmed, S.; Bidstrup, S. A.; Kohl, P. A.; Ludovice, P. J. *J. Am. Chem. Phys.* **1998**, *102*, 9783.
(29) (a) Nordman, C. E.; Schmitkos, D. L. *Acta Crystallogr.* **1965**, *18*, 765. (b) Jackson, R. L.; Strange, J. H. *Acta Crystallogr.* **1972**, *B28*, 1645.
(30) (a) Sherwood, N. *The Plastically Crystalline State, (Orientationally disordered crystals)*; John Wiley & Sons: Chichester, England, 1979. (b) Aston, J. G. In *Physics and Chemistry of Organic Solid State*; Fox, D., Labes, M. M., Weissember, A.; Eds.; Interscience Publ.: New York, 1963; Vol. 1, 543. (c) Staveley, L. A. K. *Annu. Rev. Phys. Chem.* **1962**, *13*, 351.
(31) Dominguez, L.; Enkelmann, V.; Meyer, W. H.; Wegner, G. *Polymer* **1989**, *30*, 2030.

MA0486694